Research Article | Vol. 12, No. 8 / 1 August 2021 / Biomedical Optics Express 4969
Biomedical Optics EXPRESS

Subjective measurement of the Stiles-Crawford effect with different field sizes

VINAY KUMAR NILAGIRI,[1] MARWAN SUHEIMAT,[1] ANDREW J. LAMBERT,[2] ANDREW TURPIN,[3] BRIAN VOHNSEN,[4] AND DAVID A. ATCHISON[1,*]

[1] *Institute of Health and Biomedical Innovation, School of Optometry and Vision Science, Queensland University of Technology, Brisbane, QLD, Australia*
[2] *School of Engineering and Information Technology, The University of New South Wales, Canberra, ACT, Australia*
[3] *School of Computing and Information Systems, The University of Melbourne, Melbourne, VIC, Australia*
[4] *Advanced Optical Imaging Group, School of Physics, University College Dublin, Dublin 4, Ireland*
[*] *d.atchison@qut.edu.au*

Abstract: The Stiles-Crawford effect of the first kind (SCE) is the phenomenon in which light entering the eye near the center of the pupil appears brighter than light entering near the edge. Previous investigations have found an increase in the directionality (steepness) of the effect as the testing location moves from the center of the visual field to parafoveal positions, but the effect of central field size has not been considered. The influence of field size on the SCE was investigated using a uniaxial Maxwellian system in which stimulus presentation was controlled by an active-matrix liquid crystal display. SCE directionality increased as field size increased from 0.5° to 4.7° diameter, although this was noted in four mild myopes and not in two emmetropes. The change with field size was supported by a geometric optics absorption model.

1. Introduction

The reduction in visual sensitivity when a ray of light is translated from being incident in the eye near to the pupil center and towards the periphery is known as the Stiles-Crawford effect (SCE) of the first kind [1]. The photoreceptor cones are responsible for the SCE. The most apparent contribution of the SCE to the visual system is a reduction in sensitivity to intraocular scattering of light and glare as it dampens obliquely incident light at the retina. It may also dampen aberrations causing oblique incidence on the retina [2] although for typical pupil sizes such an effect is relatively small [3–6].

Various theories attempt to explain the SCE, but the waveguide theory of photoreceptor directionality is the most widely accepted [7–10], in which cones act like waveguides that guide light near their axes better than light at oblique angles. The waveguide theory does typically not account in detail for the nonguided light, yet leaked light may trigger vision in adjacent photoreceptors as evident from electromagnetic propagation models [11,12]. As leaked rays travel largely in straight lines, Vohnsen et al. [13] proposed a geometric optics absorption model based on the fraction of overlap of light at the retina and the photoreceptor outer segments that can be applied for both Maxwellian and non-Maxwellian illuminations. The model takes into account parameters such as density, dimensions and spacing of cone outer segments and resulting variations in SCE directionality. The model was compared to experimental findings for the foveal and parafoveal regions using a constant 2.3° visual field and varying direction of gaze up to an eccentricity of 7.5° nasal and 5.0° temporal [14].

The SCE is usually fitted to a Gaussian equation

$$\eta = \eta_{max} 10^{-\rho_{10}(x-x_{max})^2} \tag{1}$$

#427834 https://doi.org/10.1364/BOE.427834
Journal © 2021 Received 14 Apr 2021; revised 7 Jul 2021; accepted 8 Jul 2021; published 16 Jul 2021

Biomedical Optics EXPRESS

where η is brightness sensitivity at pupil entry position x (in millimeters) relative to a reference position near the pupil center, η_{max} is the maximum brightness sensitivity at the pupil-entry position x_{max}, and ρ_{10} is the directionality parameter (mm^{-2}). Sometimes, ρ_e is used instead of ρ_{10} in Eq. (1), where ρ_e and ρ_{10} are related by $\rho_e = \rho_{10}\log_e 10 = 2.303\ \rho_{10}$:

$$\eta = \eta_{max} e^{-\rho_e (x - x_{max})^2} \tag{1a}$$

Other equations to describe the SCE have been proposed [15–17]. Rativa and Vohnsen [18] used a super-Gaussian equation

$$\eta = \eta_{1max} 10^{-\rho_1 (x - x_{max})^2} + \eta_{2max} 10^{-\rho_2 (x - x_{max})^4} \tag{2}$$

where variables η_{1max}, η_{2max}, ρ_1 and ρ_2, and $x_{\max}$ describe the multi-mode effects of a waveguide model. The super-Gaussian equation produces flatter central responses which improve the accuracy of the fits to data beyond that achieved with the Gaussian equation.

Factors affecting SCE directionality and peak position include wavelength [14,19,20], luminance [14,21,22], eccentricity [14,23,24], refractive errors [25,26] and aberrations [25–27], saccadic eye movements [28], and ocular diseases such as retinal detachment [29], central serous retinopathy [30], central serous choroidopathy [31], choroidal rupture [32], age-related macular changes [33,34], choroidal atrophy [35], retinitis pigmentosa [36], iris coloboma [37], and fundus ectasia [38]. Studies with artificial, decentered pupils [39,40] and congenital retinal coloboma [30] have shown evidence of active phototropism in photoreceptor alignment.

The SCE can be measured by psychophysical and objective techniques. The former usually involves subjective assessment of brightness of test and reference fields in Maxwellian illumination when test entry position is varied across the pupil [1,25,26,41]. The latter usually involves measuring illuminance of light reflected from the fundus when position of light at the pupil is varied for either inwards or outward passage through the eye [42–46], and the SCE thus determined is called the optical SCE. Directionalities reported using objective methods are often higher than those reported using psychophysical measurements, partly at least because the light passed through photoreceptors twice [42,45,47,48], but also due to the fact that objective methods analyze light that has predominantly been scattered before entering the outer segments where vision is triggered [9]. While subjective techniques are much slower than objective techniques, the latter cannot provide insight into how vision operates.

Cone density varies within and outside the foveal region [49], and the pointing direction of the group of photoreceptors towards the pupil might vary across the foveal region. Therefore, it is possible that the directionality and peak location will vary for different retinal field sizes.

The study has three aims: to investigate changes in directionality and peak location with changes in central field size, to investigate differences between fitting the Gaussian equation and the recently proposed super-Gaussian equation to results, and to determine how well the volumetric absorption model [13,14] can explain the results.

2. Methods

2.1. Participants

Right eyes of six participants with ages between 25 and 64 years were tested (Table 1). Participants were students and staff of the Queensland University of Technology. Each participant underwent an optometric examination that consisted of ocular history, visual acuity measurement, refraction, slit-lamp examination, and axial length measurements with a Lenstar LS900 (Haag-Streit, Bern, Switzerland). Each participant had best-corrected visual acuity of logMAR 0.0 and was free from ocular disease or surgery. Objective refraction was measured using an infrared autorefractor (SRW-5000; Shin-Nippon, Tokyo, Japan). Two emmetropes had +0.50 D spherical equivalent

Biomedical Optics EXPRESS

refraction and ≤ 0.5 D cylinder and four mild myopes' spherical equivalent refractions ranged between −1.25 D and −2.0 D with ≤ 0.5 D cylinder. Five of the six participants had ≥ 6.5 mm pupil size 40 minutes after dilation with one drop of 1% tropicamide (Minims, Bausch and Lomb), but the oldest participant required an additional drop of 1% phenylephrine to achieve this size. The research was approved by the Queensland University of Technology Human Research Ethics Committee. The study adhered to the tenets of the Declaration of Helsinki and informed consent was obtained from all participants.

Table 1. Refraction and axial length values of all participants. Asterisks denote emmetropic participants. Participants 2 and 5 are female, and the others are male. This distinction is made because female eyes are generally shorter than male eyes of the same refraction.

Participants	Age (yrs)	Objective refraction (Right eye)	Subjective correction on Badal scale	Axial length (mm)
1) DAA	64	–1.75/–0.50 × 110	–2.25 D	25.14
2) DS*	25	+0.75/–0.50 × 150	+0.50 D	23.08
3) PA	38	–1.75 D sphere	–1.75 D	24.50
4) MKD*	30	+0.50/–0.50 × 80	+0.50 D	22.90
5) ARC	30	–1.00/–0.50 × 175	–1.00 D	23.06
6) ASK	35	–1.50/–0.25 × 100	–1.50 D	24.32

2.2. Apparatus

The SCE was measured with a single-channel Maxwellian system (Fig. 1). White light from a fiber optic illuminator source (Intralux 6000, Volpi) passed through a 550 nm (±10 nm) green interference filter (FB550-10, Thorlabs) to illuminate 0.37 mm diameter spots (inset A) that were created using a transmission liquid crystal spatial light modulator SLM (Kopin KCM-SK01-AA CyberDisplay 1280 monochrome Evaluation kit) with a 1280 × 1024 active-matrix liquid crystal display (19.2 mm × 15.3 mm; pixel size 15 µm × 15 µm; and fill factor 94%). Each spot diameter corresponded to 25 pixels on the SLM display and the SCE system was operated over 80× luminance range.

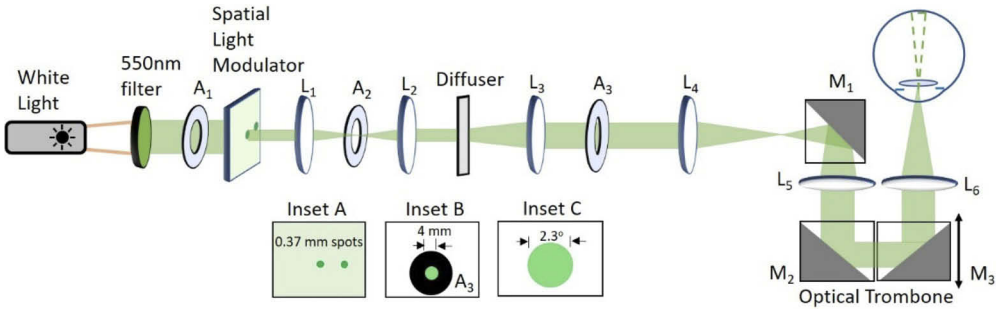

Fig. 1. Single-channel Maxwellian system. Spots created at the SLM are illuminated by a fiber optic illuminator through a 550 nm bandpass filter. A3 is a 4 mm aperture. Focal lengths of lenses are as follows: L1, L2 50 mm, L3 75 mm and L4-L6 100 mm. M1, M2 and M3 are cage-mounted mirrors. The SLM is operated as a second monitor. The eye pupil is conjugate with the SLM, and the retina is conjugate with the 4 mm diameter aperture A3 (replaced in the second part of the study by an electronic variable aperture shutter). Inset A shows the reference spot (center) and a test spot at the SLM. Inset B shows the light passing through A3. Inset C shows the participant's view when the field size is 2.3° diameter.

The 0.37 mm spots on the SLM were projected by lens combination L_1 and L_2 with unit magnification onto a diffuser that acted as a secondary display and randomized the phase. The

Biomedical Optics EXPRESS

diffuser had a Gaussian profile with a standard deviation of ~7°. The spots at the diffuser were imaged by achromatic lenses L_3-L_6, with lens combination L_3 and L_4 providing 1.33 magnification, to become 0.49 mm diameter spots at the eye entrance pupil. Aperture A_1 limited the illumination and aperture A_2 removed unwanted diffraction orders from the system, keeping only the zeroth order. The aperture A_3, conjugate with the retina, defined the angular subtense of the field (inset B). This was an electronic variable aperture (8MID 8.2-0.8-N, Standa). The aperture was connected to a computer and the aperture size was varied by changing the stepper motor values in the device software.

Mirrors M_2 and M_3 formed an optical trombone, whose position was adjusted to correct refractions of participants. As the Badal lens L_4 had a 100 mm focal length, 0.5 mm movement of the optical trombone was equivalent to 0.1 D change in refraction. The range was −3.25 D to +40 D. Refraction was measured from a ruler with diopter markings next to the trombone. The SLM was connected as a second monitor to a computer using an HDMI cable, with spots displayed using a custom-written Matlab program. Spot diameter corresponded to 25 pixels on the SLM display. The reference spot was positioned at the center of the SLM and the test spot was positioned at different positions by adjusting the x, y co-ordinates of the spot drawn with Matlab. The spots were square-wave flickered at 2 Hz (reference and test spot on for 0.25 s each) in such a way that at any instant in time the subject sees either the reference or the test field only. A keypad connected to the computer was used to record participants' responses.

Figure 2 shows the radiant flux (power) measured at the center of the pupil plane with a power meter (Thorlabs, PM100D), which has a 9.7×9.7 mm active area sensor. The grayscale setting, across the whole 8-bit SLM, was varied from 0 to 255. These values were used in a look-up table to convert the participant's thresholds to absolute power (e.g. 100 grayscale corresponds to 0.046 µW absolute power).

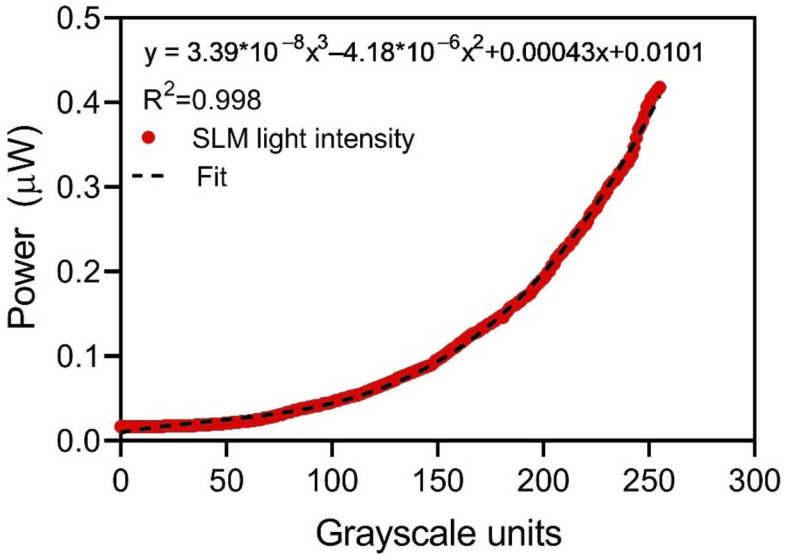

Fig. 2. Power at the pupil plane (µW) as a function of grayscale units. The solid red line shows the data and the dashed black line is the third-order polynomial fit.

Figure 3 shows the relative brightness of the test images as a function of pupil position measured at the pupil plane using a pupil camera (Pixelink PA-A741). The brightness of the test spot was highest at the center, and there was less than 5% variation out to ±3 mm. These values were used to correct the participants' absolute values. For example, if the absolute value at 1.5

Biomedical Optics EXPRESS

mm nasal pupil was set as 0.045, the value would be corrected by multiplying it by 0.98 (arrow in Fig. 3) to give a corrected value of 0.044. The correction is in all cases less than 7%.

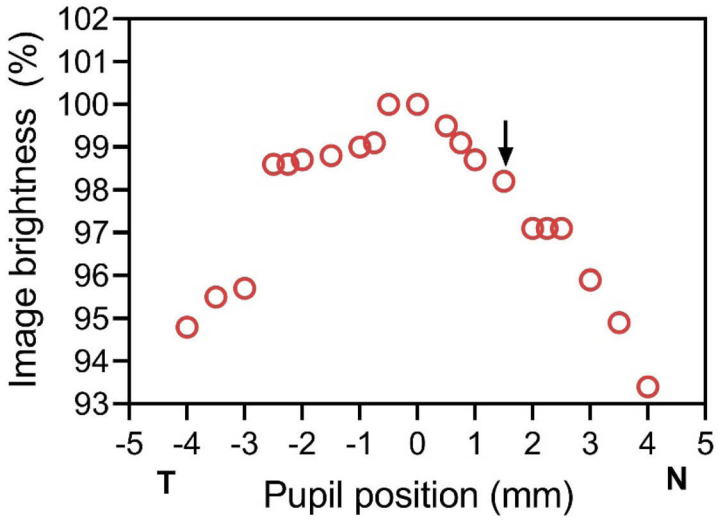

Fig. 3. Image brightness at the pupil plane as measured with a camera. The central image is assigned a value of 100%. T is temporal pupil and N is nasal pupil.

An estimation of luminance was made by comparing the Maxwellian field for the central reference spot with a 2.3° auxiliary field. An LED (Luxeon Star, Green, 530 nm) light source was used in the auxiliary system and a beam splitter allowed side by side viewing of the main and the auxiliary fields. The brightness comparison matches by one participant indicated a luminance of ≈10 cd/m^2 at the corneal plane (for a 4 mm pupil size) measured with a luminance colorimeter (BM-7A, Topcon). Participants were aligned along the instrument axis by stabilizing the head position with a bite bar mounted on an XYZ translation stage. The pupil centration was achieved by moving the participants along horizontal and vertical meridians until the illuminated field disappeared and the center position was determined from the pupil edge positions of both sides marked on a scale along both meridians. Along the Z-axis, the participant was positioned 97 mm from lens L_6 to image the spots at the entrance pupil.

2.3. Experimental procedure

Each participant's right eye was dilated before the experiment. Room illumination was lowered to avoid distractions. The left eye vision was blocked by an eye patch. The participants were given a keypad with specific keys assigned to indicate if the test field was brighter or dimmer than the reference field. Two trial runs were performed to help the participants understand the required task. A few participants experienced a shift of the test field during flicker when the test spot was presented near the edge of the pupil, especially for the smaller fields (0.46° and 1°). This made it difficult for the participants to compare the test and reference fields. This would have been because of residual refraction errors and higher-order aberrations. As necessary, the optical trombone was moved to re-establish alignment.

It was a two-alternative forced-choice test, where a participant determined if the test field was brighter or dimmer than the reference field. The test field was always accompanied by a beep sound. The output, with step-size responses and threshold values, *T*, for all positions, was saved in an Excel sheet file at the end of a run.

Biomedical Optics EXPRESS

2.3.1. Psychophysical technique

Two psychophysical techniques were investigated to measure the SCE. The **ZEST method** (Zippy Estimation of Sequential Testing) was introduced as a psychophysical testing procedure that produced unbiased estimates using a Bayesian updating procedure and *a priori* information. It has been used as the basis for spatial testing of the visual field [50–52]. Unfortunately, this resulted in long measurement times, which we attributed to a fundamental difference between perimetry and the SCE: in perimetry the majority of participants with normal peripheral vision will give similar thresholds at any location, whereas in the SCE there are considerable differences of directionality and peak sensitivity position between participants.

A two-alternative forced-choice **staircase method** was also developed and was used in the experiment. Initially, the test spot was set at 100 grayscale unit brightness. The test spot changed in 20 grayscale units at the start, lower if perceived to be brighter than the reference spot and higher if perceived to be dimmer. The step size halved for every reversal of response and rounded to the closest immediate lower number, and the threshold was taken as the grayscale level at the presentation that would be given after the fourth reversal (Fig. 4). Thirteen pupil positions, including the pupil center, were tested randomly in the horizontal meridian of the pupil in 0.5 mm steps to ±3 mm from the pupil center. Testing time was 8–13 min per run. The output, with step-size responses and thresholds for all positions, was saved in an Excel sheet file at the end of a run.

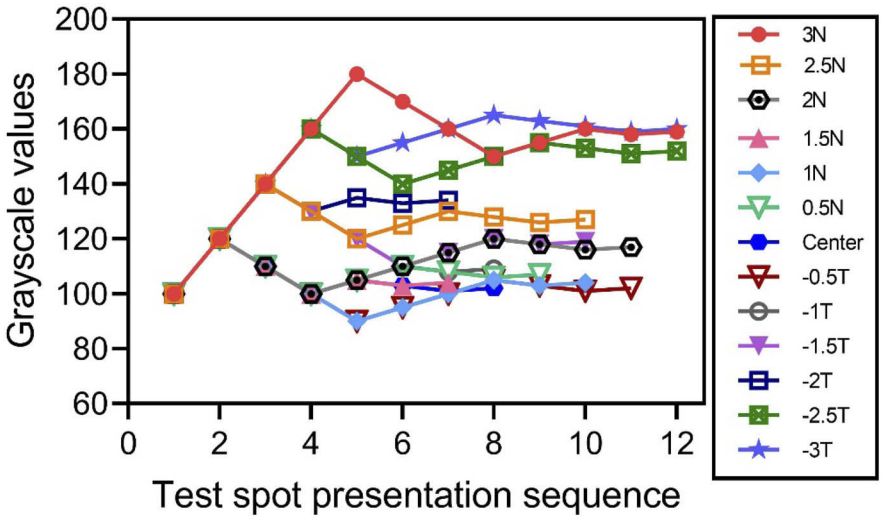

Fig. 4. A participant's responses for the stair-case method at 13 positions in the pupil. N is nasal pupil and T is temporal pupil.

2.3.2. Measuring the SCE using different field sizes

We aimed for multiple concentric field sizes from central fovea to parafoveal field size as the cone density and shape varies significantly in this range. Five field sizes $\theta = 0.46°$, 1.0°, 2.3°, 3.5° and 4.7° were used by changing the aperture size to 0.8 mm, 1.7 mm, 4.0 mm, 6.1 mm and 8.0 mm, respectively. All participants were tested first with 2.3° field and then with other field sizes (lower to higher) from 0.46° to 4.7°. Three runs were made for each field size.

Biomedical Optics EXPRESS

2.3.3. Conversion of threshold values to visibility and numerical fitting of data

Measured threshold values (section 2.3.2) were converted to visibility = $1/T$ and normalized before fitting to Eqs. (1) and (2). For the Gaussian fits to Eq. (1), the maximum sensitivity value was normalized to $\eta_{max} = 1$ (Table 2, top). The super-Gaussian fits using Eq. (2) were restricted to have ρ_1 and x_{max} the same as for the Gaussian fit and $\eta_{1max} = \eta_{2max} = 0.5$ (Table 2, bottom). More sophisticated super-Gaussian fits were tried, such as to allow both ρ_1 and ρ_2 to vary and to have unequal amplitudes such that $\eta_{2max} = 1 - \eta_{1max}$. However, improvement in the fittings were marginal and sometimes the parameters were not significantly different from zero. Fitting was done with SigmaPlot version 14 (Systat Software).

Table 2. Gaussian (G) and equal amplitude super-Gaussian (s-G) coefficients for the fits in Fig. 5. SE represents standard error.

Panel	Fit	η_{max}		ρ (mm^{-2}) (SE)		x_{max} (mm)	Adjusted R^2
a)	G fit	+1.00		+0.028 (0.0029)		–0.231	0.86
b)	G fit	+1.00		+0.034 (0.0028)		+0.193	0.91
c)	G fit	+1.00		+0.037 (0.0021)		–0.034	0.95
		η_{1max}	η_{2max}	ρ_1 (mm^{-2})	ρ_2 (mm^{-4}) (SE)	x_{max} (mm)	Adjusted R^2
a)	s-G fit	+0.50	+0.50	+0.028	+0.0042 (0.0008)	–0.231	0.90
b)	s-G fit	+0.50	+0.50	+0.034	+0.0052 (0.0008)	+0.193	0.94
c)	s-G fit	+0.50	+0.50	+0.037	+0.0057 (0.0008)	–0.034	0.95

The visibility values were also compared to volumetric absorption data determined as the intersection volume for a cylinder of light representative of the Maxwellian illumination with individual cylindrical cone outer segments with a diameter $d = 2\mu$m but variable density σ and outer segment length L representative of the different retinal eccentricities assuming hexagonal packing and a foveal peak cone density of 160,000/mm^2. The geometrical intersection volume was determined using COMSOL following the same procedure as described in Refs. [13] and [14]. Pupil position of the SCE was related to retinal angle of incidence using the measured ocular axial length of each subject. The parameters of each volumetric fit were altered manually by optimizing the R-squared value.

3. Results

Figure 5 shows selected examples of SCE data for field sizes of (a) 0.46°, (b) 1.0°, and (c) 3.5°, together with fitted curves and simulated volumetric overlap data. The quality of fits improved with an equal-amplitude super-Gaussian over the standard Gaussian SCE for all participants; on average adjusted R-squared values improved by 3%.

The volumetric data, similar to the super-Gaussian fits flattened the central response and provided slight improvements. The volumetric data were based on histology estimates of the exponentially decreasing cone density at increased eccentricity [49,53] and approximate outer-segment dimensions where the outer-segment length has the strongest impact [14]. The measured axial length of each subject was used to relate angle to pupil point of entry. Nevertheless, for the remainder of this analysis we resorted to the standard SCE Gaussian fit in Eq. (1), as this eases comparison with existing values in the literature.

Figure 6 shows the mean (±SD) Gaussian directionalities across runs, for each participant, plotted as a function of field size. The directionality for each participant was obtained from the fitting function to the data of each run. The directionality increased consistently with field size for the four mild myopes (DA, PA, ARC and ASK), but the two emmetropes (DS and MKD) did not show a similar trend. The peak position was on the nasal side for four participants and on the temporal side for two participants.

Biomedical Optics EXPRESS

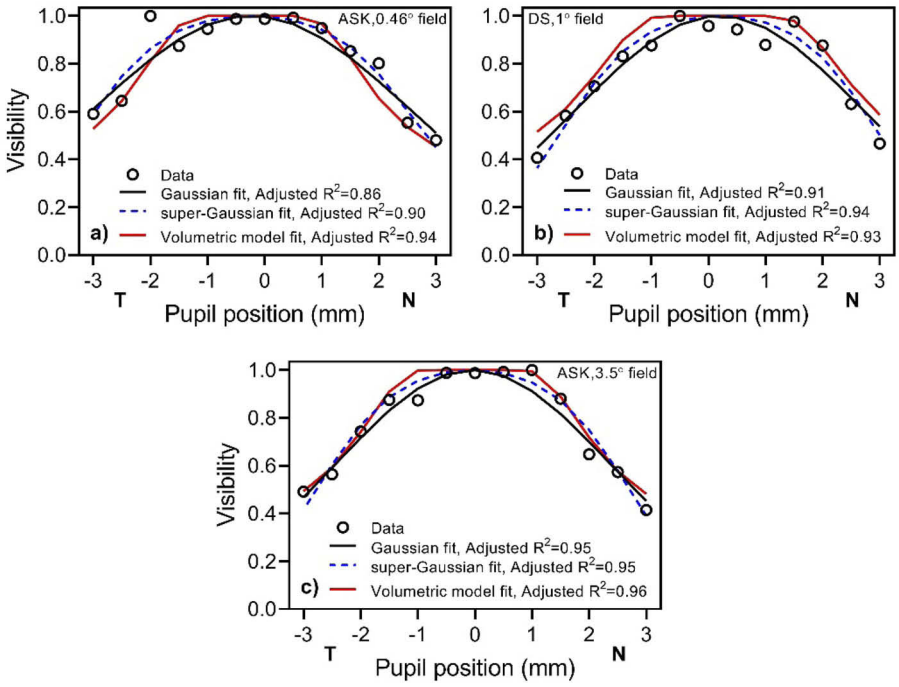

Fig. 5. Examples of SCE data, their Gaussian and equal amplitude-super-Gaussian fits, unequal amplitude super-Gaussian fits and volumetric fits and adjusted R-squared values. a) participant ASK, 0.46° field, b) participant DS, 1 ° field and c) participant ASK, 3.5 ° field. Table 2 has the parameters of the G and s-G fits. The volumetric fits were made for individual cylindrical outer segments with diameter $d = 2\mu m$ and having densities σ and length L of: (a) 160,000/mm^2 and 40μm; (b) 80,000/mm^2 and 33.7μm; (c) 20,000/mm^2 and 40μm, respectively, with 30% M cones.

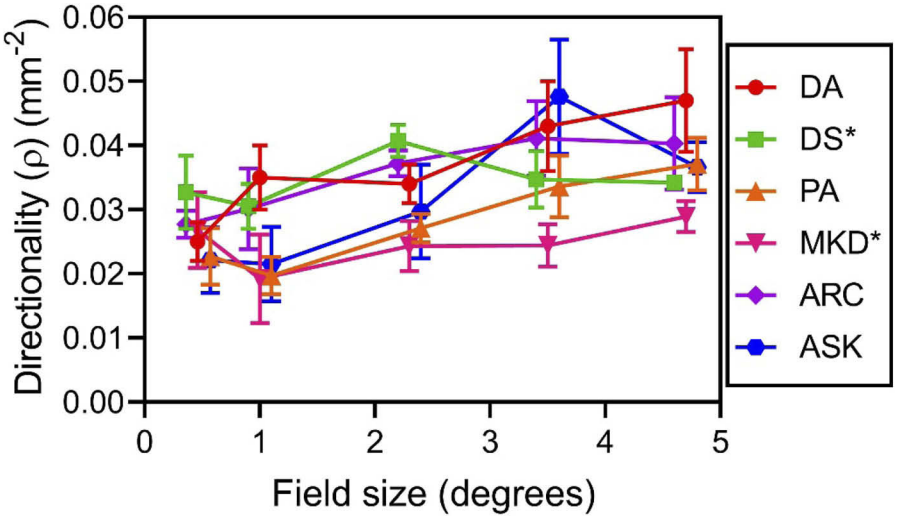

Fig. 6. Directionality (ρ) fits as a function of field size for participants. Error bars are ±1SDs of three runs. Four participants' data are displaced by ±0.05° on the X-axis for clarity. The asterisks indicate the emmetropic participants.

Biomedical Optics EXPRESS

The mean directionalities obtained from three runs per field size and the best-selected run of those three runs per field size of each participant were compared. The choice of the best run was determined as the one with the smallest x_{max} offset as this allows for the most symmetric, high-quality fit. The regression fits showed a similar trend.

Figure 7 shows the best selected directionalities of participants plotted as a function of field size, together with the linear fit ($R^2 = 0.37$, p = 0.0003). The directionalities of myopes and emmetropes were averaged separately (Fig. 8). All corrected myopes showed increasing directionality with increasing field size with an average of 0.02 to 0.05 mm^{-2} for 0.46° to 4.7° fields ($R^2 = 0.60$, p

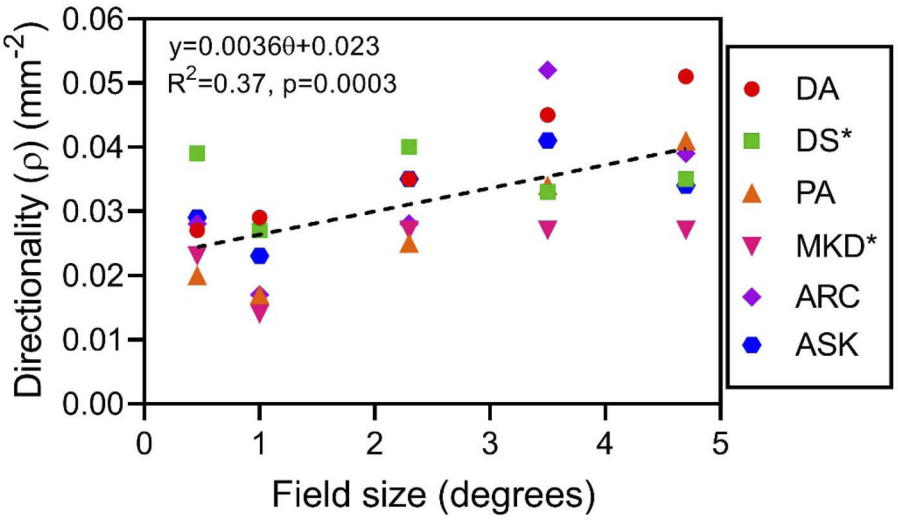

Fig. 7. Directionalities (ρ) of participants as a function of field size. Each data point is the best-selected data from the three runs of each participant. The fit is for 35 points. The asterisks indicate the emmetropic participants.

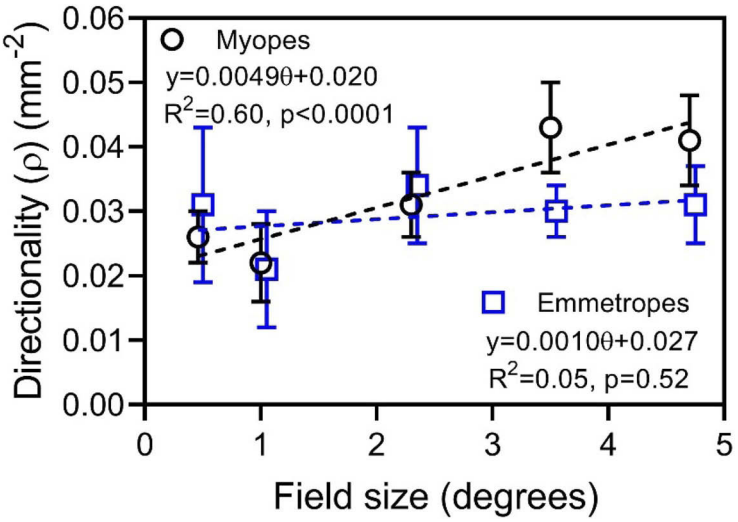

Fig. 8. Directionality (ρ) as a function of field size for myopic and emmetropic groups. Error bars are ±1 SDs. As for Fig. 7, fits are based on individual directionalities. For clarity, the emmetropes' data are displaced by 0.05° to the right.

Biomedical Optics EXPRESS

<0.0001), respectively, but the two emmetropes did not exhibit such a trend and the determined directionality remained practically constant across all field sizes.

4. Discussion

The SCE measured with a uniaxial Maxwellian system incorporating a SLM provided directionality values in good agreement with the previous literature [14,26,54]. Across all participants the directionality increased with the field size by 1.9 times from 0.46° to 4.7° (Fig. 7), but with a minor reduction at 1° field size that might relate to the transition from the 0.35 mm foveola to the fovea. The increase with field size was evident in four corrected myopes, but not in two corrected emmetropes (Fig. 8). If any minor refractive error remained in the system it could offset the determined directionality parameter [25,26] in an equal manner for both emmetropes and mild myopes and it would be small. The most apparent increase in directionality with field size beyond 1° occurred for the most myopic subjects (DA, PA and ASK) although one case showed an unexpected peak at 3.5°. In any case, the investigation dividing subjects into the refractive groups was lacking in statistical strength (power analysis: $\alpha = 0.05$, power = 0.8, sample required n = 8 in each group) and further testing would be necessary to further explore any possible differences. There is evidence that myopes have reduced linear cone density at the fovea, due to the stretching of the posterior eyeball, than emmetropes [55]. These may produce changes in the directionality and the peak location that were not apparent in emmetropes.

Martins and Vohnsen [14] reported on parafoveal SCE measurements for a fixed 2.3° field size with blue, green and red light and found increased directionality at 2.5° when compared to the fovea beyond which a reduction was observed at up to 7.5°. A study by Choi et al. [24] showed increasing directionality from fovea out to 15° retinal eccentricity. Our finding of increasing directionality up to 4.7° for a concentric field can be considered to be in reasonable agreement with those of Martins and Vohnsen [14], where the directionality was measured at different eccentricities but we increased the field size to cover the same extent.

One of the limitations of fitting a Gaussian function to the data was that the fits are driven by the outermost data points in the pupil for a few runs of the participants. To overcome this, the data were fitted also with super-Gaussian functions. The accuracy of the fits improved in nearly all cases as previously reported by Rativa and Vohnsen [18]. The improvement was relatively modest at about 0.03–0.04 increase in adjusted R-squared values.

The value of the volumetric absorption model [13,14] can be appreciated in Fig. 5 where it can be seen to make good fits to the selected data. To examine the implications in more detail, additional examples are shown in Fig. 9 for myopic subject DA where the dependence on outer segment length and cone density is explored in more detail with respect to field size. The SCE directionality measured with a constant field size tends to be lowest in myopic eyes [24–26]. Three cases of cone outer segment length L of 35, 40 and 45μm were examined along with densities σ 160,000/mm^2, 40,000/mm^2, and 20,000/mm^2, respectively, and 30% M cones as representative for eccentricities of 0.47°, 2.3°, and 4.7°, respectively. These values were derived at using representative cone foveal and parafoveal parameters reported in the literature [49,53]. The quality of the fits is summarized in Table 3. The volumetric model reproduces the plateau observed near the pupil center as also suggested by the super-Gaussian fits (Fig. 5).

As Fig. 9 shows, the impact of outer segment length is vital in the quality of the fits. Outer segment diameter and cone density play lesser roles but may explain some of the variations observed. The volumetric data provide an attractive physical basis from which to interpret the directionality and visibility data that the Gaussian or super-Gaussian models lack. However, more histological knowledge about photoreceptor densities and dimensions are still required to tune the absorption model more accurately to the psychophysical data. This is also suggested by the adjusted R-squared values found. This will be done in future work.

Biomedical Optics EXPRESS

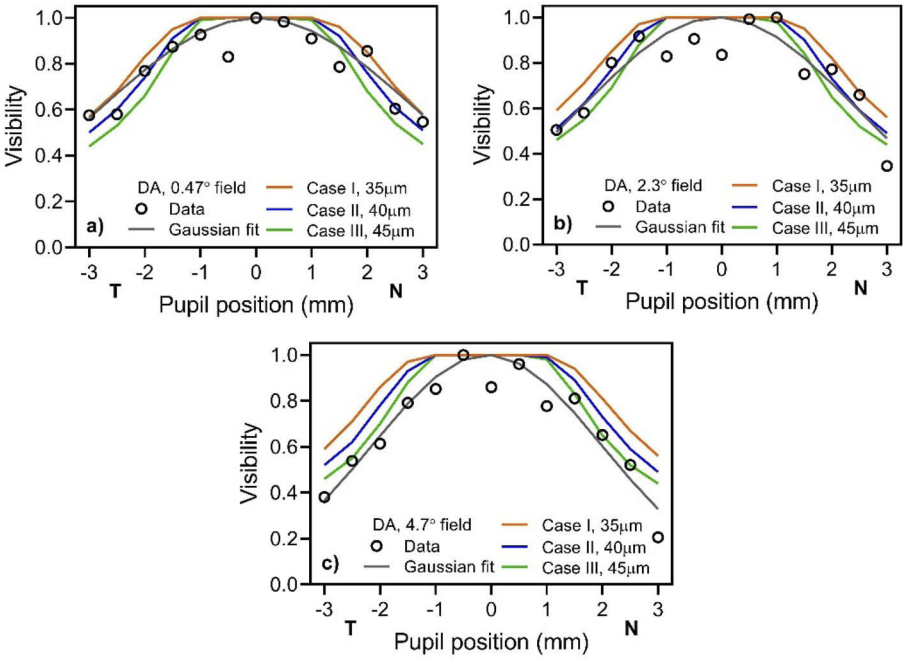

Fig. 9. Volumetric integration model [13,14] results when overlapping a cylinder of light (representative of the Maxwellian illumination) across outer segments representative of foveal and parafoveal cones when compared with visibility data for subject DA with field sizes of (a) 0.47°, (b), 2.3°, and (c) 4.7°. The curves show cylindrical outer segment lengths of 35, 40 and 45 µm with diameter 2µm and assumed cone densities of (a) 160,000 cones/mm^2, (b) 40,000/mm^2 and (c) 20,000/mm^2. 30% M cones was assumed.

Table 3. Comparison between adjusted R-squared values determined with Gaussian SCE and volumetric fits for the data in Fig. 9.

Panel	Field size	Gaussian fit	Case I, 35µm	Case II, 40µm	Case III, 45µm
a)	0.47° field	0.77	0.83	0.83	0.80
b)	2.3° field	0.75	0.81	0.77	0.72
c)	4.7° field	0.89	0.88	0.84	0.85

5. Conclusions

The SCE directionality increases with the field size out to 4.7° with, in a small sample, a different trend for mild myopes than for emmetropes. Some theoretical support for this was provided by a volumetric integration model that showed differences in characteristic directionality and also confirmed the observed often "flat" central appearance of the SCE function that led to the introduction of the super-Gaussian model. The super-Gaussian fitting function, that retained the ρ value and peak of the Gaussian function, fits the data slightly better than the Gaussian fitting function in nearly all cases due to the flatter central response.

Funding. Australian Research Council (DP190103069).

Acknowledgements. We thank all our participants for their time.

Disclosures. The authors report no conflicts of interest and have no proprietary interest in any of the materials mentioned in this article.

Biomedical Optics EXPRESS

Data availability. Data underlying the results presented in this paper are not publicly available at this time but may be obtained from the authors upon reasonable request.

References

1. W. S. Stiles and B. H. Crawford, "The luminous efficiency of rays entering the eye pupil at different points," Proc. R. Soc. Lond. B **123**(830), 90–118 (1937).
2. B. Vohnsen, "Photoreceptor waveguides and effective retinal image quality," J. Opt. Soc. Am. A **24**(3), 597–607 (2007).
3. D. A. Atchison, D. H. Scott, A. Joblin, and G. Smith, "Influence of Stiles–Crawford effect apodization on spatial visual performance with decentered pupils," J. Opt. Soc. Am. A **18**(6), 1201–1211 (2001).
4. D. A. Atchison, D. H. Scott, N. C. Strang, and P. Artal, "Influence of Stiles–Crawford apodization on visual acuity," J. Opt. Soc. Am. A **19**(6), 1073–1083 (2002).
5. D. A. Atchison and D. H. Scott, "Contrast sensitivity and the Stiles–Crawford effect," Vision Res. **42**(12), 1559–1569 (2002).
6. D. A. Atchison, S. Marcos, and D. H. Scott, "The influence of the Stiles-Crawford peak location on visual performance," Vision Res. **43**(6), 659–668 (2003).
7. W. Wright and J. Nelson, "The relation between the apparent intensity of a beam of light and the angle at which the beam strikes the retina," Proc. Phys. Soc. **48**(3), 401–405 (1936).
8. G. T. Di Francia, "Retina cones as dielectric antennas," J. Opt. Soc. Am. **39**(4), 324 (1949).
9. B. Vohnsen, I. Iglesias, and P. Artal, "Guided light and diffraction model of human-eye photoreceptors," J. Opt. Soc. Am. A **22**(11), 2318–2328 (2005).
10. J. M. Enoch, "Wave-guide modes in retinal receptors," Science **133**(3461), 1353–1354 (1961).
11. B. Vohnsen, "Directional sensitivity of the retina: a layered scattering model of outer-segment photoreceptor pigments," Biomed. Opt. Express **5**(5), 1569–1587 (2014).
12. A. Meadway and L. C. Sincich, "Light propagation and capture in cone photoreceptors," Biomed. Opt. Express **9**(11), 5543–5565 (2018).
13. B. Vohnsen, A. Carmichael, N. Sharmin, S. Qaysi, and D. Valente, "Volumetric integration model of the Stiles-Crawford effect of the first kind and its experimental verification," J. Vis. **17**(12), 18 (2017).
14. A. Carmichael Martins and B. Vohnsen, "Directional light-capture efficiency of the foveal and parafoveal photoreceptors at different luminance levels: an experimental and analytical study," Biomed. Opt. Express **10**(8), 3760–3772 (2019).
15. J. M. Enoch, "Summated response of the retina to light entering different parts of the pupil," J. Opt. Soc. Am. **48**(6), 392–405 (1958).
16. A. Safir, L. Hyams, and J. Philpot, "Movement of the Stiles-Crawford effect," Invest. Ophthalmol. Vis. Sci. **9**, 820–825 (1970).
17. P. Moon and D. E. Spencer, "On the Stiles-Crawford effect," J. Opt. Soc. Am. A **34**(6), 319–329 (1944).
18. D. Rativa and B. Vohnsen, "Single-and multimode characteristics of the foveal cones: the super-Gaussian function," J. Mod. Opt. **58**(19-20), 1809–1816 (2011).
19. W. S. Stiles, "The luminous efficiency of monochromatic rays entering the eye pupil at different points and a new colour effect," Proc. R. Soc. Lond. B **123**(830), 90–118 (1937).
20. B. Lochocki, D. Rativa, and B. Vohnsen, "Spatial and spectral characterisation of the first and second Stiles–Crawford effects using tuneable liquid-crystal filters," J. Mod. Opt. **58**(19-20), 1817–1825 (2011).
21. W. S. Stiles, "The directional sensitivity of the retina and the spectral sensitivities of the rods and cones," Proc. R. Soc. Lond. B **127**(846), 64–105 (1939).
22. B. Crawford, "The luminous efficiency of light entering the eye pupil at different points and its relation to brightness threshold measurements," Proc. R. Soc. Lond. B **124**(834), 81–96 (1937).
23. J. M. Enoch and G. Hope, "Directional sensitivity of the foveal and parafoveal retina," Invest. Ophthalmol. Vis. Sci. **12**, 497–503 (1973).
24. S. S. Choi, L. F. Garner, and J. M. Enoch, "The relationship between the Stiles–Crawford effect of the first kind (SCE-I) and myopia," Oph Phys Optics **23**(5), 465–472 (2003).
25. N. Singh, D. A. Atchison, S. Kasthurirangan, and H. Guo, "Influences of accommodation and myopia on the foveal Stiles–Crawford effect," J. Mod. Opt. **56**(20), 2217–2230 (2009).
26. A. Carmichael Martins and B. Vohnsen, "Analysing the impact of myopia on the Stiles-Crawford effect of the first kind using a digital micromirror device," Ophthalmic Physiol. Opt. **38**(3), 273–280 (2018).
27. D. A. Atchison and D. H. Scott, "The Stiles–Crawford effect and subjective measurement of aberrations," Vision Res. **42**(9), 1089–1102 (2002).
28. W. Richards, "Saccadic suppression," J. Opt. Soc. Am. **59**(5), 617–623 (1969).
29. F. Fankhauser, J. Enoch, and P. Cibis, "Receptor orientation in retinal pathology: a first study," Am. J. Ophthalmol. **52**(5), 767–783 (1961).
30. C. Dunnewold, "On the Campbell and Stiles–Crawford effects and their clinical importance. Rijksuniversiteit Utrecht," (Doctoral dissertation, Utrecht, 1964).
31. V. C. Smith, J. Pokorny, and K. R. Diddie, "Color matching and Stiles-Crawford effect in central serous choroidopathy," J. Opt. Soc. Am. A **5**(12), 2113 (1988).

Biomedical Optics EXPRESS

32. E. C. Campos, H. E. Bedell, J. M. Enoch, and C. R. Fitzgerald, "Retinal receptive field-like properties and Stiles-Crawford effect in a patient with a traumatic choroidal rupture," Doc Ophthalmol. **45**(2), 381–395 (1978).
33. V. C. Smith, J. Pokorny, and K. R. Diddie, "Color matching and the Stiles–Crawford effect in observers with early age-related macular changes," J. Opt. Soc. Am. A **5**(12), 2113–2121 (1988).
34. C. R. Fitzgerald, J. M. Enoch, E. C. Campos, and H. E. Bedell, "Comparison of visual function studies in two cases of senile macular degeneration," Albrecht von Graefes Arch. Klin. Ophthalmol. **210**(2), 79–91 (1979).
35. H. E. Bedell, J. M. Enoch, and C. R. Fitzgerald, "Photoreceptor orientation: a graded disturbance bordering a region of choroidal atrophy," Arch. Ophthalmol. **99**(10), 1841–1844 (1981).
36. D. G. Birch, M. A. Sandberg, and E. L. Berson, "The Stiles-Crawford effect in retinitis pigmentosa," Invest. Ophthalmol. Vis. Sci. **22**, 157–164 (1982).
37. J. E. Bailey, V. Lakshminarayanan, and J. M. Enoch, "Photoreceptor orientation in iris coloboma," Optom. Vis. Sci. **71**(2), 120–124 (1994).
38. V. Lakshminarayanan, J. E. Bailey, and J. M. Enoch, "Photoreceptor orientation and alignment in nasal fundus ectasia," Optom. Vis. Sci. **74**(12), 1011–1018 (1997).
39. R. A. Applegate and A. Bonds, "Induced movement of receptor alignment toward a new pupillary aperture," Invest. Ophthalmol. Vis. Sci. **21**, 869–872 (1981).
40. M. J. Collins, F. Yi, B. A. Davis, and H. J. McNeill, "Rapid changes in the Stiles Crawford function in response to a decentred aperture," Invest. Ophthalmol. Vis. Sci. **60**, 5944 (2019).
41. B. Lochocki and B. Vohnsen, "Uniaxial flicker analysis of the psychophysical Stiles–Crawford effects," J. Mod. Opt. **64**(4), 347–356 (2017).
42. J.-M. Gorrand and F. Delori, "A reflectometric technique for assessing photoreceptor alignment," Vision Res. **35**(7), 999–1010 (1995).
43. S. A. Burns, S. Wu, F. Delori, and A. E. Elsner, "Direct measurement of human-cone-photoreceptor alignment," J. Opt. Soc. Am. A **12**(10), 2329–2338 (1995).
44. A. Roorda and D. R. Williams, "Optical fiber properties of individual human cones," J. Vis. **2**(5), 4 (2002).
45. H. J. Morris, L. Blanco, J. L. Codona, S. L. Li, S. S. Choi, and N. Doble, "Directionality of individual cone photoreceptors in the parafoveal region," Vision Res. **117**, 67–80 (2015).
46. D. Rativa and B. Vohnsen, "Analysis of individual cone-photoreceptor directionality using scanning laser ophthalmoscopy," Biomed. Opt. Express **2**(6), 1423–1431 (2011).
47. P. Delint, T. Berendschot, and D. Van Norren, "Local photoreceptor alignment measured with a scanning laser ophthalmoscope," Vision Res. **37**(2), 243–248 (1997).
48. W. Gao, B. Cense, Y. Zhang, R. S. Jonnal, and D. T. Miller, "Measuring retinal contributions to the optical Stiles-Crawford effect with optical coherence tomography," Opt. Express **16**(9), 6486–6501 (2008).
49. C. A. Curcio, K. R. Sloan, R. E. Kalina, and A. E. Hendrickson, "Human photoreceptor topography," J. Comp. Neurol. **292**(4), 497–523 (1990).
50. P. E. King-Smith, S. S. Grigsby, A. J. Vingrys, S. C. Benes, and A. Supowit, "Efficient and unbiased modifications of the QUEST threshold method: theory, simulations, experimental evaluation and practical implementation," Vision Res. **34**(7), 885–912 (1994).
51. A. Turpin, A. M. McKendrick, C. A. Johnson, and A. J. Vingrys, "Development of efficient threshold strategies for frequency doubling technology perimetry using computer simulation," Invest. Ophthalmol. Vis. Sci. **43**, 322–331 (2002).
52. A. Turpin, A. M. McKendrick, C. A. Johnson, and A. J. Vingrys, "Performance of efficient test procedures for frequency-doubling technology perimetry in normal and glaucomatous eyes," Invest. Ophthalmol. Vis. Sci. **43**, 709–715 (2002).
53. R. F. Spaide and C. A. Curcio, "Anatomical correlates to the bands seen in the outer retina by optical coherence tomography: literature review and model," Retina **31**(8), 1609–1619 (2011).
54. R. A. Applegate and V. Lakshminarayanan, "Parametric representation of Stiles–Crawford functions: normal variation of peak location and directionality," J. Opt. Soc. Am. A **10**(7), 1611–1623 (1993).
55. Y. Wang, N. Bensaid, P. Tiruveedhula, J. Ma, S. Ravikumar, and A. Roorda, "Human foveal cone photoreceptor topography and its dependence on eye length," Elife **8**, e47148 (2019).